On the Silicides $EuIr_2Si_2$ and Lu_5Si_3

Ute Ch. Rodewald[a], Birgit Heying[a], Dirk Johrendt[b], and Rainer Pöttgen[a]

[a] Institut für Anorganische und Analytische Chemie, Westfälische Wilhelms-Universität Münster, Corrensstraße 36, D-48149 Münster, Germany
[b] Department Chemie und Biochemie, Ludwig-Maximilians-Universität München, Butenandtstraße 5 – 13 (Haus D), D-81377 München, Germany

Reprint requests to R. Pöttgen. E-mail: pottgen@uni-muenster.de

Z. Naturforsch. **59b,** 969 – 974 (2004); received June 18, 2004

Dedicated to Professor Kurt O. Klepp on the occasion of his 60th birthday

$EuIr_2Si_2$ was synthesized from the elements in a sealed tantalum tube in a water-cooled sample chamber of an induction furnace. Lu_5Si_3 was obtained by arc-melting of the elements. Both silicides were investigated by X-ray powder and single crystal diffraction: $BaAl_4$ type, $I4/mmm$, $a = 407.4(1)$, $c = 1010.8(7)$ pm, $wR2 = 0.0492$, 134 F^2 values, 9 variables for $EuIr_2Si_2$ and Mn_5Si_3 type, $P6_3/mcm$, $a = 820.0(1)$, $c = 614.2(1)$ pm, $wR2 = 0.0511$, 311 F^2 values and 12 variables for Lu_5Si_3. The iridium and silicon atoms in $EuIr_2Si_2$ build up a three-dimensional $[Ir_2Si_2]$ network with Ir–Si and Si–Si interactions. The europium atoms fill cages within the network. The metal-rich silicide Lu_5Si_3 contains columns of face-sharing, empty Lu_6 octahedra and *isolated* silicon atoms in a distorted tri-capped trigonal prismatic coordination. Chemical bonding in these silicides is briefly discussed.

Key words: Silicide, Crystal Structure, Solid State Synthesis, Chemical Bonding

Introduction

During our recent phase analytical investigations of rare-earth metal (*RE*)-transition metal (*T*)-silicides and germanides [1 – 6], we obtained good quality single crystals of the silicides Lu_5Si_3 and $EuIr_2Si_2$. So far both compounds had only been characterized on the basis of X-ray powder data.

Lu_5Si_3 with the hexagonal Mn_5Si_3 type structure has first been synthesized by Gladyshevskii and Krypyakevich by arc-melting [7, 8]. Later on, Smith *et al.* [9] and Mayer and Shidlovsky [10] confirmed these results and they also investigated the silicides Lu_5Si_4 [9] and Lu_5Si_3C [10], where the octahedral voids formed by the lutetium atoms are filled by silicon or carbon, respectively. The standard enthalpy of formation of Lu_5Si_3 has been studied by Topor and Kleppa [11], and the temperature dependence of the electrical resistivity can be interpreted by a combination of the phonon contribution and an interband scattering term [12].

The intermediate valence system $EuIr_2Si_2$ (tetragonal $BaAl_4$ type) was first obtained by Chevalier *et al.* [13, 14]. The europium valence changes from $4f^{6.2}$ at 4.2 K to $4f^{6.7}$ at 290 K, as determined from ^{151}Eu Mössbauer spectroscopic data. The valence fluctuation behavior of $EuIr_2Si_2$ has been reported also by Vijayaraghavan *et al.* [15 – 17].

Herein we report on single crystal studies and an evaluation of chemical bonding of Lu_5Si_3 and $EuIr_2Si_2$.

Experimental Section

Synthesis

Starting materials for the synthesis of Lu_5Si_3 and $EuIr_2Si_2$ were ingots of europium and lutetium (Johnson Matthey), iridium powder (*ca.* 200 mesh, Degussa-Hüls), and silicon lumps (Wacker), all with purities better than 99.9%. The crystals of Lu_5Si_3 were first obtained from a ternary sample of the initial composition 2La:3Lu:4Si. We have then prepared a pure binary sample. In a first step, small pieces of the lutetium lumps were arc-melted to a small button (*ca.* 400 mg) under an argon atmosphere of *ca.* 600 mbar [18]. The argon was purified over titanium sponge (870 K), silical gel, and molecular sieves. The premelting of lutetium reduces a shattering during the strongly exothermic reaction with silicon. The lutetium button was subsequently mixed with small pieces of silicon in the ideal

5 : 3 atomic ratio and arc-melted three times in order to achieve homogeneity. The weight loss after the various melting steps was smaller than 0.5 weight-%.

Due to the low boiling temperature of europium (1870 K) and the high melting temperature of iridium (2683 K) [19], a synthesis of $EuIr_2Si_2$ via arc-melting is not adequate. A substantial loss of europium can occur in this quasi-open system. A well crystallized polycrystalline sample containing several well-shaped single crystals of $EuIr_2Si_2$ was obtained from a sample with the initial composition 1Eu:1Ir:1Si, when we tried to synthesize the equiatomic silicide [6]. Europium pieces, iridium powder, and powdered silicon were sealed in a small tantalum tube (*ca.* 1 cm^3) under an argon pressure of 800 mbar in the atomic ratio 1:1:1. The tantalum tube was placed in a special water-cooled quartz sample chamber [20] in an induction furnace (Hüttinger Elektronik, Freiburg, Typ TIG 5.0/300), and first heated to *ca.* 1400 K for 5 min. The strongly exothermic reaction between the three elements was discernible through a heat flash. The tube was subsequently annealed for another 2 h at *ca.* 1070 K and finally quenched to room temperature by switching off the power supply. The sample was mechanically broken off the tube. No reaction of the crucible material with the sample could be detected. A small drop of europium was visible at the upper, colder cap of the tantalum tube. Since the X-ray powder pattern revealed $EuIr_2Si_2$ and a small amount of $EuIrSi_3$ [13], some elemental europium remained in the sample.

Powders and the polycrystalline samples of Lu_5Si_3 and $EuIr_2Si_2$ are stable in air over months. Some excess europium that remained at the grain boundaries slightly hydrolyzed with the humidity of the air. Polycrystalline pieces and single crystals of Lu_5Si_3 and $EuIr_2Si_2$ are silvery with metallic lustre. Powders are dark gray.

EDX analyses

The Lu_5Si_3 and $EuIr_2Si_2$ single crystals were coated with a carbon film and analyzed in a Leica 420 I scanning electron microscope by energy dispersive X-ray analyses using EuF_3, LuF_3, iridium, and SiO_2 as standards. The compositions of the crystals (16 ± 4 at.-% Eu : 44 ± 4 at.-% Ir : 40 ± 4 at.-% Si and 51 ± 6 at.-% Lu : 49 ± 6 at.-% Si) determined by the EDX analyses were in good agreement with those obtained from the structure refinements. No impurity elements heavier than sodium could be detected. The relatively high standard deviations arise from the irregular surface of the crystals.

X-ray film data and structure refinements

The samples were routinely characterized through their Guinier powder patterns using Cu Kα_1 radiation and α-quartz ($a = 491.30$, $c = 540.46$ pm) as an internal standard. The Guinier camera was equipped with an image plate system (Fujifilm, BAS-1800). The lattice parameters (Table 1) were refined from the Guinier powder data. To ensure correct indexing, the observed patterns were compared with data calculated [21] using the atomic positions obtained from the structure refinements. Our lattice parameters for Lu_5Si_3 and $EuIr_2Si_2$ compare well with those reported in literature [7 – 10, 13, 14]. Also the powder and the single crystal lattice parameters agree well.

Table 1. Crystal data and structure refinement for $EuIr_2Si_2$ and Lu_5Si_3.

Empirical formula	$EuIr_2Si_2$	Lu_5Si_3
Formula weight	592.54 g/mol	959.12 g/mol
Unit cell dimensions	$a = 407.4(1)$ pm	$a = 820.0(1)$ pm
	$c = 1010.8(7)$ pm	$c = 614.2(1)$ pm
	$V = 0.1678$ nm^3	$V = 0.3577$ nm^3
Pearson symbol	t*I*10	h*P*16
Structure type	$BaAl_4$	Mn_5Si_3
Space group	$I4/mmm$	$P6_3/mcm$
Formula units per cell	$Z = 2$	$Z = 2$
Calculated density	11.73 g/cm^3	8.91 g/cm^3
Crystal size	$20 \times 25 \times 65$ μm^3	$20 \times 20 \times 30$ μm^3
Transmission ratio (max/min)	4.04	1.82
Absorption coefficient	98.0 mm^{-1}	68.7 mm^{-1}
$F(000)$	490	794
Detector distance	60 mm	60 mm
Exposure time	30 min	20 min
ω range; increment	0 – 180°, 1.0°	0 – 180°, 1.0°
Integration parameters A, B, EMS	16.0, 2.0, 0.05	15.0, 4.5, 0.016
θ Range for data coll.	4° to 35°	4° to 35°
Range in *hkl*	±6, ±6, ±16	±13, ±13, ±9
Total no. of reflections	1190	5004
Independent reflections	134 ($R_{int} = 0.1005$)	311 ($R_{int} = 0.1133$)
Reflections with $I > 2\sigma(I)$	134 ($R_\sigma = 0.0432$)	287 ($R_\sigma = 0.0312$)
Data / parameters	134 / 9	311 / 12
Goodness-of-fit on F^2	0.865	1.152
Final *R* indices	$R1 = 0.0209$	$R1 = 0.0200$
$[I > 2\sigma(I)]$	$wR2 = 0.0492$	$wR2 = 0.0494$
R Indices (all data)	$R1 = 0.0209$	$R1 = 0.0241$
	$wR2 = 0.0492$	$wR2 = 0.0511$
Extinction coefficient	0.041(2)	0.0016(2)
Largest diff. peak	3.13	1.55
and hole	and −3.29 e/Å^3	and −1.51 e/Å^3

Irregularly-shaped single crystals of Lu_5Si_3 and $EuIr_2Si_2$ were selected from the mechanically crushed samples. They were first investigated by Laue photographs on a Buerger precession camera which was equipped with an image plate system (Fujifilm, BAS-1800). Two suitable single crystals were then used for the intensity data collections on a Stoe IPDS-II diffractometer with graphite monochromatized Mo-K$_\alpha$ radiation in oszillation mode. A numerical absorption correction was applied to the data. Details for the data collections and evaluations are listed in Table 1.

Analyses of the data sets revealed the space groups $P6_3/mcm$ (Lu_5Si_3) and $I4/mmm$ ($EuIr_2Si_2$), in agreement

Atom	Wyckoff position	*x*	*y*	*z*	U_{11}	U_{22}	U_{33}	U_{12}	U_{eq}
$EuIr_2Si_2$ (space group *I*4/*mmm*)									
Eu	2*a*	0	0	0	71(2)	U_{11}	95(3)	0	79(2)
Ir	4*d*	0	1/2	1/4	51(2)	U_{11}	95(3)	0	66(2)
Si	4*e*	0	0	0.3739(3)	75(6)	U_{11}	98(10)	0	83(5)
Lu_5Si_3 (space group *P*6$_3$/*mcm*)									
Lu1	6*g*	0.24124(4)	0	1/4	79(2)	68(2)	130(2)	34(1)	93(1)
Lu2	4*d*	2/3	1/3	0	102(2)	U_{11}	65(2)	51(1)	90(1)
Si	6*g*	0.6045(3)	0	1/4	66(7)	90(10)	131(12)	45(5)	93(5)

Table 2. Atomic coordinates and anisotropic displacement parameters (pm^2) for $EuIr_2Si_2$ and Lu_5Si_3. U_{eq} is defined as one third of the trace of the orthogonalized U_{ij} tensor. $U_{13} = U_{23} = 0$.

Table 3. Interatomic distances (pm) in the structures of $EuIr_2Si_2$ and Lu_5Si_3, calculated with the lattice parameters obtained from the Guinier powder data.

$EuIr_2Si_2$			**Lu_5Si_3**		
Eu:	8 Si	315.0(1)	Lu1:	2 Si	283.2(2)
	8 Ir	324.6(1)		1 Si	297.8(3)
	2 Si	377.9(3)		2 Si	332.1(1)
Ir:	4 Si	239.1(2)		2 Lu1	342.6(1)
	4 Ir	288.1(1)		4 Lu2	353.0(1)
	4 Eu	324.6(1)		4 Lu1	365.3(1)
Si:	4 Ir	239.1(2)	Lu2:	6 Si	294.9(1)
	1 Si	255.0(4)		2 Lu2	307.1(1)
	4 Eu	315.0(1)		6 Lu1	353.0(1)
	1 Eu	377.9(3)	Si:	2 Lu1	283.2(2)
				4 Lu2	294.9(1)
				1 Lu1	297.8(3)
				2 Lu1	332.1(1)

with the X-ray powder data [7 – 10, 13, 14]. The starting atomic positions were deduced from automatic interpretations of direct methods with SHELXS-97 [22], and both structures were refined with SHELXL-97 [23] (full-matrix least-squares on F^2) with anisotropic displacement parameters for all sites. As a check for the correct composition, the occupancy parameters were refined in a separate series of least-squares cycles. All sites were fully occupied within two standard deviations, and in the final cycles the ideal occupancies were assumed again. Final difference Fourier syntheses revealed no significant residual peaks. The refined positional parameters and interatomic distances are listed in Tables 2 and 3. Further details on the structure refinements are available.*

Electronic structure calculations

Self-consistent band structure calculations were performed using the LMTO-method in its scalar-relativistic version (program TB-LMTO-ASA) [24]. Detailed descriptions are given elsewhere [25, 26]. Reciprocal space integrations were performed with the tetrahedron method using 1335 *k*-points for $EuIr_2Si_2$ and 95 *k*-points for Lu_5Si_3 within the irreducible wedges of the Brillouin zones [27]. The basis sets consisted of $6s/6p/5d$ for Lu and Eu, $6s/6p/5d/5f$ for Ir and $3s/3p/3d$ for Si. The $5f$ orbitals of Ir and the $3d$ orbitals of Si were downfolded [28] and the Lu/Eu $4f$ orbitals treated as core states for convergence reasons. In order to achieve space filling within the atomic sphere approximation, interstitial spheres are introduced to avoid too large overlap of the atom-centered spheres. The empty spheres positions and radii were calculated automatically. We did not allow overlaps of more than 15% for any two atom centered spheres. The COHP method was used for the bond analysis [29]. COHP gives the energy contributions of all electronic states for a selected bond. The values are negative for bonding and positive for antibonding interactions. With respect to the COOP diagrams, we plot –COHP(E) to get positive values for bonding states.

Discussion

The unit cell of $EuIr_2Si_2$ is shown in Fig. 1. The iridium and silicon atoms build up a three-dimensional $[Ir_2Si_2]$ network in which the europium atoms fill large cages formed by eight silicon and eight iridium atoms. The Ir–Si distances within the $[Ir_2Si_2]$ network are 239 pm, slightly smaller than the sum of the covalent radii of 244 pm. In isotypic α-$CeIr_2Si_2$ the Ir–Si dis-

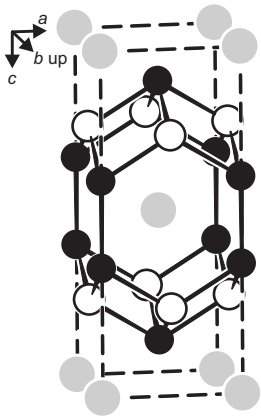

Fig. 1. Unit cell of the tetragonal $EuIr_2Si_2$ structure. Europium, iridium, and silicon atoms are drawn as light gray, open, and filled circles, respectively. The three-dimensional $[Ir_2Si_2]$ network is emphasized.

*Details may be obtained from: Fachinformationszentrum Karlsruhe, D-76344 Eggenstein-Leopoldshafen (Germany), by quoting the Registry No's. CSD–414146 ($EuIr_2Si_2$) and CSD–414147 (Lu_5Si_3).

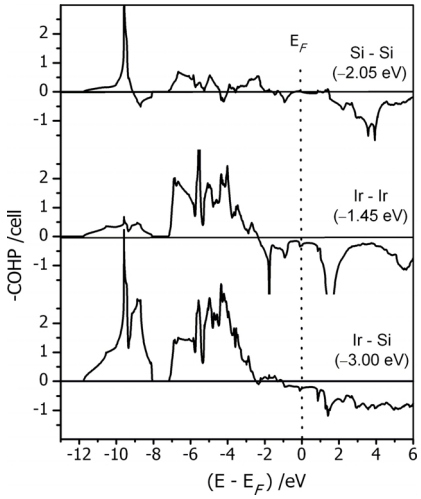

Fig. 2. Crystal Orbital Hamiltonian Population (COHP) diagrams of the Ir−Si, Ir−Ir and Si−Si bonds in $EuIr_2Si_2$. Numbers in parentheses are the COHP bonding energy values ICOHP in eV/bond.

tance is 241 pm [19]. The Si–Si distance of 255 pm in $EuIr_2Si_2$ is significantly longer than the Si–Si distance of 235 pm in elemental silicon [30]. We can thus assume only weak Si–Si bonding character, similar to the situation in the silicides $RE_2RE'_3Si_4$ [5]. In this context it should be remembered that there exist definitely two branches for the family of 1:2:2 compounds: the $BaZn_2P_2$ branch with isolated phosphorus atoms and the $BaAl_4$ / $ThCr_2Si_2$ branch where Al–Al and Si–Si bonds (or X–X bonds in general) occur [31, 32]. $EuIr_2Si_2$ belongs to the $BaAl_4$ / $ThCr_2Si_2$ branch with weak Si–Si bonds.

This is in agreement with LMTO band structure calculations. Fig. 2 shows COHP diagrams of the Si–Si, Ir–Ir and Ir–Si bonds in $EuIr_2Si_2$. The Si−Si bond is relatively weak though almost only Si–Si bonding states are occupied up to E_F. The integrated COHP bonding (ICOHP) energy is −2.05 eV/bond. The by far strongest bonds are the Ir–Si linkages the ICOHP energy of which is −3.00 eV/bond. Significant metal-metal bonding within the square nets is typical for this branch of the $ThCr_2Si_2$-type. This is also confirmed by the Ir–Ir COHP, which shows strong bonding states occupied between −7 and −3 eV, followed by some weak antibonding levels between −3 eV and the Fermi level. The ICOHP energy is −1.45 eV/bond, thus the Ir–Ir bonds are weaker than the Si–Si bonds, but there are only two of the latter in the unit cell, whereas eight Ir–Ir bonds exist. Nonetheless, the largest part of the total

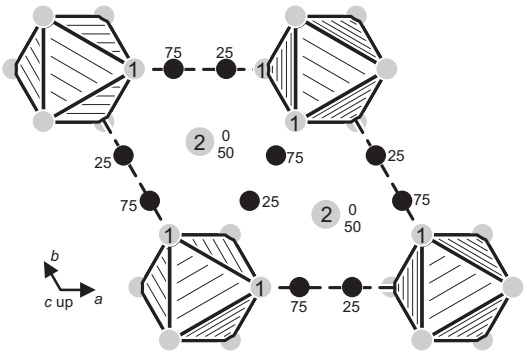

Fig. 3. Projection of the Lu_5Si_3 structure onto the *xy* plane. Lutetium and silicon atoms are drawn as light gray and black circles, respectively. The empty $Lu1_6$ octahedra are emphasized. Atom designations and the heights of the atoms in hundredths are indicated.

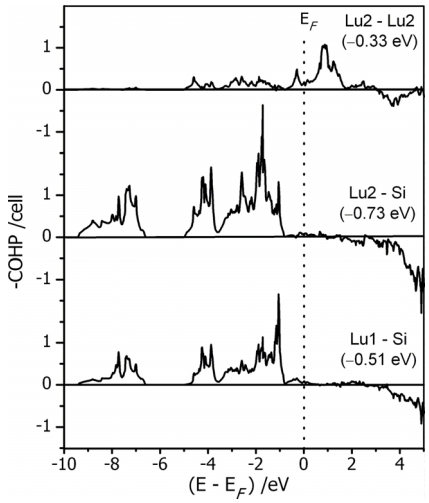

Fig. 4. Crystal Orbital Hamiltonian Population (COHP) diagrams of the Lu–Si and the short Lu–Lu bonds in Lu_5Si_3. Contributions of different bonds according to Table 2 were added up. Numbers in parentheses are the COHP bonding energy values ICOHP in eV/bond.

bonding energy of $EuIr_2Si_2$ results from the 16 Ir–Si bonds in the unit cell.

The bonding situation in binary Lu_5Si_3 with hexagonal Mn_5Si_3 type [33, 34] structure is different. Lu_5Si_3 belongs to the group of metal-rich silicides and consequently we observe a variety of Lu–Lu interactions. The silicon atoms are *isolated*, with nine lutetium neighbors in a distorted tri-capped trigonal prismatic coordination (Fig. 3). The Si–Lu distances range from 283 to 332 pm, longer than the sum of the covalent radii of 273 pm.

The Lu1 atoms are arranged around the 6_3 screw axis at $0\,0\,z$. They build up columns of empty, face-sharing $Lu1_6$ octahedra. The Lu1–Lu1 distances of these octahedra range from 343 to 365 pm, close to the average Lu–Lu distance of 347 pm in *hcp* lutetium [30]. A remarkable feature of the Lu_5Si_3 structure is the extremely short Lu2–Lu2 distance of 307 pm. This distance corresponds to half the *c* lattice parameter.

Figure 4 shows the COHP diagrams of selected bonds in Lu_5Si_3. The short Lu2–Lu2 distances correspond to Lu–Lu bonds, generated by the Lu-5*d* orbitals. Only a small part of the bonding states are occupied, and consequently the Lu2–Lu2 bonding energy of -0.33 eV/bond is rather small. On the other side, this small occupation of Lu-5d orbitals is suggestive for ionized Lu^{3+}. The Si-3*p* orbitals are surely completely filled, and we can assume a formulation $(5Lu^{3+})^{15+}(3Si^{4-})^{12-}(3e^-)^{3-}$ for this metallic compound. The main part of the total bonding energy comes from the Lu–Si bonds, as expected. The COHP calculation reveals that the average ICOHP bond energy is larger for the Lu2–Si (-0.73 eV/bond) than for the Lu1–Si bonds (-0.51 eV/bond). This is in agreement with the longer average bond distances of 305.7 pm for Lu1–Si compared with the six equal Lu2–Si bonds of 294.9 pm.

Acknowledgments

We thank H.-J. Göcke for the work at the scanning electron microscope. This work was financially supported by the Deutsche Forschungsgemeinschaft.

[1] D. Niepmann, R. Pöttgen, Intermetallics **9**, 313 (2001).
[2] R. Mishra, R. Pöttgen, G. Kotzyba, Z. Naturforsch. **56b**, 463 (2001).
[3] R. Mishra, R.-D. Hoffmann, R. Pöttgen, Z. Anorg. Allg. Chem. **627**, 1787 (2001).
[4] U. Ch. Rodewald, R. Pöttgen, Solid State Sci. **5**, 487 (2003).
[5] U. Ch. Rodewald, B. Heying, D. Johrendt, R.-D. Hoffmann, R. Pöttgen, Z. Naturforsch. **59b**, 174 (2004).
[6] B. Heying, U. Ch. Rodewald, M. Valldor, R.-D. Hoffmann, R. Mishra, R. Pöttgen, Monatsh. Chem., in press.
[7] E. I. Gladyshevskii, P. I. Krypyakevich, J. Struct. Chem. **5**, 853 (1964).
[8] E. I. Gladyshevskii, Izv. Akad. Nauk. SSSR, Neorg. Mater. **1**, 868 (1965).
[9] G. S. Smith, A. G. Tharp, Q. Johnson, Acta Crystallogr. **22**, 940 (1967).
[10] I. Mayer, I. Shidlovsky, Inorg. Chem. **8**, 1240 (1969).
[11] L. Topor, O. J. Kleppa, J. Less-Common Met. **167**, 91 (1990).
[12] F. Canepa, S. Cirafici, F. Merlo, A. Palenzona, J. Magn. Magn. Mater. **118**, 182 (1993).
[13] X. Z. Wang, B. Lloret, L. Ng. Wee, B. Chevalier, J. Etourneau, P. Hagenmuller, Rev. Chim. Minér. **22**, 711 (1985).
[14] B. Chevalier, J. M. D. Coey, B. Lloret, J. Etourneau, J. Phys. C: Solid State Phys. **19**, 4521 (1986).
[15] S. Patil, R. Nagarajan, L. C. Gupta, R. Vijayaraghavan, B. D. Padalia, Solid State Commun. **63**, 955 (1987).
[16] S. Patil, R. Nagarajan, L. C. Gupta, B. D. Padalia, R. Vijayaraghavan, Physica B: Condens. Matter **163**, 340 (1990).
[17] S. Patil, R. Nagarajan, L. C. Gupta, B. D. Padalia, R. Vijayaraghavan, Solid State Commun. **76**, 1173 (1990).
[18] R. Pöttgen, Th. Gulden, A. Simon, GIT-Laborfachzeitschrift **43**, 133 (1999).
[19] J. Emsley, The Elements, Oxford University Press, Oxford (1999).
[20] D. Kußmann, R.-D. Hoffmann, R. Pöttgen, Z. Anorg. Allg. Chem. **624**, 1747 (1998).
[21] K. Yvon, W. Jeitschko, E. Parthé, J. Appl. Crystallogr. **10**, 73 (1977).
[22] G. M. Sheldrick, SHELXS-97, Program for the Determination of Crystal Structures, University of Göttingen, Germany (1997).
[23] G. M. Sheldrick, SHELXL-97, Program for Crystal Structure Refinement, University of Göttingen, Germany (1997).
[24] O. K. Andersen, O. Jepsen, Tight-Binding LMTO Vers. 4.7, Max-Planck-Institut für Festkörperforschung, Stuttgart (1994).
[25] O. Jepsen, M. Snob, O. K. Andersen, Linearized Band Structure Methods and its Applications, Springer Lecture Notes, Springer-Verlag, Berlin (1987).
[26] H. L. Skriver, The LMTO Method, Springer-Verlag, Berlin (1984).
[27] O. K. Andersen, O. Jepsen, Solid State Commun. **9**, 1763 (1971).
[28] W. R. L. Lambrecht, O. K. Andersen, Phys. Rev. **B34**, 2439 (1986).
[29] R. Dronskowski, P. Blöchl, J. Phys. Chem. **97**, 8617 (1993).
[30] J. Donohue, The Structures of the Elements, Wiley, New York (1974).

[31] D. Schmitz, W. Bronger, Z. Anorg. Allg. Chem. **553**, 248 (1987).
[32] H. G. von Schnering, R. Türck, W. Hönle, K. Peters, E.-M. Peters, R. Kremer, J.-H. Chang, Z. Anorg. Allg. Chem. **628**, 2772 (2002).
[33] K. Åmark, B. Boren, A. Westgren, Svensk Kem. Tidskr. **48**, 273 (1936).
[34] B. Aronsson, Acta Chem. Scand. **14**, 1414 (1960).